Recent cryogenic EM imaging of the PSD in intact synapses revealed a regular row of electron-dense material running parallel to the postsynaptic membrane at ~6-nm spacings, by our measurement (*32*). Although the nature of this array is not yet known, it could correspond to a view of a Shank organized sheet looking either down the ends of the fibers (~6-nm spacings due to fiber interdigitation). The proposed sheet structure, with radially projecting protein interaction domains, appears to be an ideal architecture for a protein that must contact both membrane and cytoplasmic components at a two-dimensional cell surface. The ability of Zn^{2+} to aid the organization of the Shank sheet raises the possibility that Zn^{2+} ions, which are released during neuronal activity (*33*–*35*), could directly modulate the PSD structure by regulating the assembly of Shank SAM domains.

References and Notes

1. H. J. Carlisle, M. B. Kennedy, *Trends Neurosci.* **28**, 182 (2005).
2. M. B. Kennedy, *Science* **290**, 750 (2000).
3. K. W. Li *et al.*, *J. Biol. Chem.* **279**, 987 (2004).
4. J. Peng *et al.*, *J. Biol. Chem.* **279**, 21003 (2004).
5. A. I. Matus, D. H. Taff-Jones, *Proc. R. Soc. London Ser. B* **203**, 135 (1978).
6. M. Sheng, M. J. Kim, *Science* **298**, 776 (2002).
7. A. Matus, *Science* **290**, 754 (2000).
8. P. M. Okamoto, C. Gamby, D. Wells, J. Fallon, R. B. Vallee, *J. Biol. Chem.* **276**, 48458 (2001).
9. T. Bresler *et al.*, *J. Neurosci.* **24**, 1507 (2004).
10. M. D. Ehlers, *Trends Neurosci.* **25**, 64 (2002).
11. E. Kim, M. Sheng, *Nat. Rev. Neurosci.* **5**, 771 (2004).
12. T. M. Boeckers, J. Bockmann, M. R. Kreutz, E. D. Gundelfinger, *J. Neurochem.* **81**, 903 (2002).
13. S. Lim *et al.*, *J. Biol. Chem.* **274**, 29510 (1999).
14. B. Qualmann *et al.*, *J. Neurosci.* **24**, 2481 (2004).
15. J. G. Valtschanoff, R. J. Weinberg, *J. Neurosci.* **21**, 1211 (2001).
16. F. G. Wouterlood, T. Bockers, M. P. Witter, *J. Neurosci. Methods* **128**, 129 (2003).
17. G. Roussignol *et al.*, *J. Neurosci.* **25**, 3560 (2005).
18. F. Qiao, J. U. Bowie, *Sci. STKE* **2005**, re7 (2005).
19. J. Behlke, D. Labudde, O. Ristau, *Eur. Biophys. J.* **30**, 411 (2001).
20. C. D. Thanos, K. E. Goodwill, J. U. Bowie, *Science* **283**, 833 (1999).
21. C. A. Kim *et al.*, *EMBO J.* **20**, 4173 (2001).
22. S. Naisbitt *et al.*, *Neuron* **23**, 569 (1999).
23. T. M. Boeckers *et al.*, *J. Neurochem.* **92**, 519 (2005).
24. Single-letter abbreviations for the amino acid residues are as follows: A, Ala; C, Cys; D, Asp; E, Glu; F, Phe; G, Gly; H, His; I, Ile; K, Lys; L, Leu; M, Met; N, Asn; P, Pro; Q, Gln; R, Arg; S, Ser; T, Thr; V, Val; W, Trp; and Y, Tyr.
25. Materials and methods are available as supporting material on *Science* Online.
26. H. H. Jan, I. T. Chen, Y. Y. Tsai, Y. C. Chang, *J. Neurochem.* **83**, 525 (2002).
27. C. J. Chang *et al.*, *Chem. Biol.* **11**, 203 (2004).
28. D. S. Auld, *Biometals* **14**, 271 (2001).
29. L. A. Finney, T. V. O'Halloran, *Science* **300**, 931 (2003).
30. F. Vanhaecke, M. Resano, L. Moens, *Anal. Bioanal. Chem.* **374**, 188 (2002).
31. J. A. Caruso, M. Montes-Bayon, *Ecotoxicol. Environ. Saf.* **56**, 148 (2003).
32. B. Zuber, I. Nikonenko, P. Klauser, D. Muller, J. Dubochet, *Proc. Natl. Acad. Sci. U.S.A.* **102**, 19192 (2005).
33. Y. Li, C. J. Hough, S. W. Suh, J. M. Sarvey, C. J. Frederickson, *J. Neurophysiol.* **86**, 2597 (2001).
34. J. H. Weiss, S. L. Sensi, *Trends Neurosci.* **23**, 365 (2000).
35. D. W. Choi, J. Y. Koh, *Annu. Rev. Neurosci.* **21**, 347 (1998).

36. Coordinates have been deposited in the Protein Data Bank with accession codes 2F3N and 2F44. This work was supported by NIH grant no. RO1 CA081000 to J.U.B., an NIH Cellular and Molecular Biology Training Grant to M.K.B., by the Deutsche Forschungsgemeinschaft (grants SFB 497/B8 and SFB 426/A1) to T.M.B. and E.D.G., and by the State of Baden-Württemberg (grant 1423/74) to T.M.B. J.U.B. is a Leukemia and Lymphoma Society Scholar.

Supporting Online Material

www.sciencemag.org/cgi/content/full/311/5760/531/DC1
Materials and Methods
References

17 August 2005; accepted 28 December 2005
10.1126/science.1118995

Design and Evolution of New Catalytic Activity with an Existing Protein Scaffold

Hee-Sung Park,[1] Sung-Hun Nam,[1] Jin Kak Lee,[2]* Chang No Yoon,[2] Bengt Mannervik,[3] Stephen J. Benkovic,[4] Hak-Sung Kim[1]†

The design of enzymes with new functions and properties has long been a goal in protein engineering. Here, we report a strategy to change the catalytic activity of an existing protein scaffold. This was achieved by simultaneous incorporation and adjustment of functional elements through insertion, deletion, and substitution of several active site loops, followed by point mutations to fine-tune the activity. Using this approach, we were able to introduce β-lactamase activity into the αβ/βα metallohydrolase scaffold of glyoxalase II. The resulting enzyme, evMBL8 (evolved metallo β-lactamase 8), completely lost its original activity and, instead, catalyzed the hydrolysis of cefotaxime with a $(k_{cat}/K_m)^{app}$ of 1.8×10^2 (mole/liter)$^{-1}$ second^{-1}, thus increasing resistance to *Escherichia coli* growth on cefotaxime by a factor of about 100.

Enzymes with new functions targeted at practical applications have long been a goal of protein engineering, and advances have been made with methods involving structure-based rational design or directed evolution (*1*–*4*). These approaches allow improvement of specific enzyme characteristics such as folding and stability (*5*), substrate specificity and enantioselectivity (*6*), and catalytic activity (*7*), but the design of enzymes with new functions remains a challenge. Computational design of proteins has had notable successes, culminating in Hellinga and co-workers' report (*8*) introducing triose phosphate isomerase activity into a noncatalytic ribose-binding protein. However, a lack of understanding of structure-function relations continues to hinder rational design, and methods relying on accumulation of point mutations remain desirable.

We have used an approach designated SIAFE (simultaneous incorporation and adjustment of functional elements), in conjunction with directed evolution, to introduce new catalytic activity into an existing scaffold. A schematic illustration of the SIAFE process is presented in fig. S1. SIAFE consists of insertion, deletion, and substitution of gene segments in addition to the conventional directed evolution method of accumulating point mutations, mimicking natural protein evolution (*9*, *10*). Functional elements (catalytic and substrate-binding elements) that constitute the active site are designed on the basis of sequence, mechanistic, and structural information and are incorporated into a template scaffold in a programmed and combinatorial manner. Using this approach, we generated β-lactamase activity from the glyoxalase II αβ/βα metallohydrolase scaffold.

The αβ/βα four-layer sandwich scaffold is proposed to have diverged extensively during evolution to give rise to a superfamily of metallohydrolase enzymes that are distributed over Eukarya, Archaea, and Bacteria. This superfamily catalyzes a variety of diverse reactions and includes metallo β-lactamase (MBL), glyoxalase II (GlyII), flavoprotein, arylsulfatase, type II polyketide synthase, β-CASP family, cytidine monophosphate (CMP)-N-acetylneuraminate hydroxylase, and phosphodiesterase (*11*). GlyII and MBL catalyze unrelated metabolic reactions, but their marginal structural similarity and conserved metal-binding site suggest that they are evolutionarily related (*12*) so that they present a typical example of the differentiation of a progenitor scaffold. GlyII (EC 3. 1. 2. 6) is involved in the hydrolysis of the thiolester bond of S-D-lactoylglutathione (Fig. 1A), a critical step in the conversion of cytotoxic 2-oxoaldehyde into 2-hydroxycarboxylic acids that occurs in the cyto-

[1]Department of Biological Sciences, Korea Advanced Institute of Science and Technology, 373-1, Kusung-Dong, Yusung-Gu, Daejon 305-701, Korea. [2]Bioanalysis and Biotransformation Research Center, Korea Institute of Science and Technology, Post Office Box 131, Cheongryang, Seoul 130-650, Korea. [3]Department of Biochemistry, Uppsala University, Biomedical Center, Box 576, SE-751 23 Uppsala, Sweden. [4]Department of Chemistry, The Pennsylvania State University, 104 Chemistry Building, University Park, PA 16802, USA.

*Present address: Nanormics Inc., Seoul, Korea.
†To whom correspondence should be addressed. Email: hskim76@kaist.ac.kr

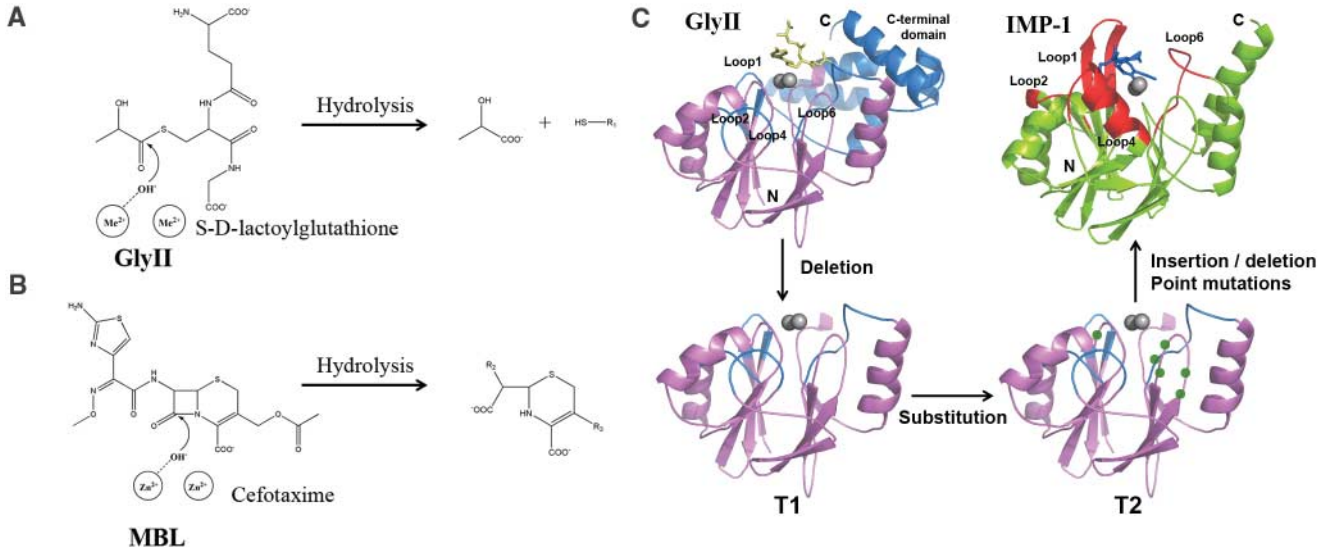

Fig. 1. Strategy for generation of MBL activity from GlyII. Catalytic mechanisms of (**A**) GlyII and (**B**) MBL. (**C**) Reconstruction of the active site of GlyII for generation of IMP-1 activity with the SIAFE process. As the first step, the C-terminal domain was deleted to produce template T1, and the catalytic elements (marked by green circles) were substituted to yield T2. Substrate-binding elements consisting of predesigned functional loops with different lengths and sequences were inserted, and random point mutations were induced for further adjustment. Functional loops constituting the active site of IMP-1 [Protein Data Bank (PDB) entry, 1DDK)] are shown in red, and the corresponding loops of GlyII (PDB entry, 1QH5) are in blue. The C-terminal domain to be deleted is shown in blue. Substrates for GlyII and IMP-1, S-(N-hydroxy-N-bromophenylcarbamoyl)glutathione and cefotaxime, are shown in yellow and blue, respectively

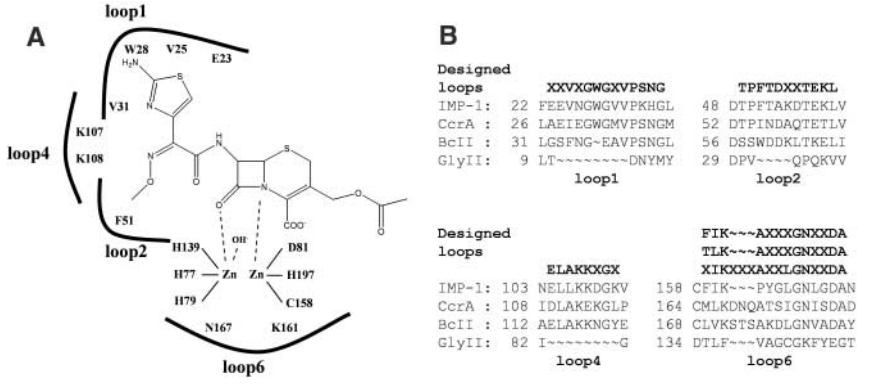

Fig. 2. Design of the MBL active site architecture. (**A**) Schematic diagram of the IMP-1 active site. Metal coordination and the active site pocket are shown. (**B**) Newly designed loops from the sequences of MBL family enzymes. IMP-1, MBL from *P. aeruginosa*; CcrA, MBL from *Bacteroides fragilis*; BcII, MBL from *Bacillus cereus* (*13*); GlyII, GlyoxalaseII from human (*12*).

plasm (*12*), whereas MBL (EC 3. 5. 2. 6) catalyzes the hydrolysis of the β-lactam amide bond to inactivate β-lactam antibiotics in the periplasmic space (Fig. 1B), giving rise to bacterial resistance against β-lactam antibiotics (*13*).

Human GlyII (260 amino acids, 29 kD) and IMP-1 (228 amino acids, 25 kD), an MBL family member from *Pseudomonas aeruginosa*, share a low sequence identity (13% for regions between 1 and 177 of GlyII and regions between 14 and 201 of IMP-1), but the overall folds are similar (Fig. 1C). Both contain αβ/βα sandwich structures and binuclear metal ions essential to the hydrolysis reaction. The active sites, however, differ in metal coordination and substrate binding. Typically, IMP-1 contains two Zn ions linked by a hydroxide molecule. Zn1 has tetrahedral coordination (H77, H79, and H139), and Zn2 has trigonal bipyramidal coordination (D81, C158, and H197) (*14*). GlyII, on the other hand, can have various metal ions, such as iron, manganese, or zinc, in its binuclear site (*15*). Metal 1 in GlyII is coordinated with three histidine residues similarly to Zn1 in MBL. However, for metal 2, C158 is replaced by D134, and H59 acts as an additional ligand (*12*). There are no common characteristics to substrate binding between GlyII and IMP-1. The IMP-1 substrate-binding site is composed mainly of loops 1, 2, and 6. Loop 1 (E23, V25, W28, and V31) and loop 2 (F51) constitute a hydrophobic pocket for β-side chain substituents of antibiotics (Fig. 2A) (*16*). Loop 6 contains K161 and N167, which are crucial for binding and activation of the β-lactam substrate during catalysis (*17*). Preliminary studies revealed that mutations (K107E and K108E) in IMP-1 loop 4 caused specific activity to decrease by a factor of about 100, which suggests that this loop plays some role in β-lactam binding or catalysis from a distance. In GlyII, loop 4 (K143 and Y145) and the C-terminal helical domain (Y175, R248, and K252) are implicated in binding (*12*). Thus, the distinct catalytic reactions derive from different active site architectures.

On the basis of sequence, mechanistic, and structural information, we used the SIAFE process to reconstruct the active site of GlyII (Fig. 1C) to bind and catalyze the hydrolysis of a typical substrate for MBL, cefotaxime. The C-terminal glutathione-binding domain of GlyII (residues 178 to 260) sterically prevents binding of a new substrate. Therefore, the first step was the deletion of this binding domain to create a template T1. The loss of critical substrate-binding elements caused the T1 template to lose all GlyII activity. Catalytic and substrate-binding elements for the new active site were designed in the next step. The catalytic elements of metallohydrolase superfamily enzymes mainly consist of metal-binding ligands and residues for stabilization of metal coordination. The T1 template was substituted with the following catalytic elements to produce T2: H59C and D134C for Zn affinity, A106Y, insertion of glycine between T107 and P108, S112T, and G113D for Zn stabilization (*18*). We also constructed a new active site pocket based on the sequence alignment of respective loops in MBL family enzymes. For loop 6, there is consider-

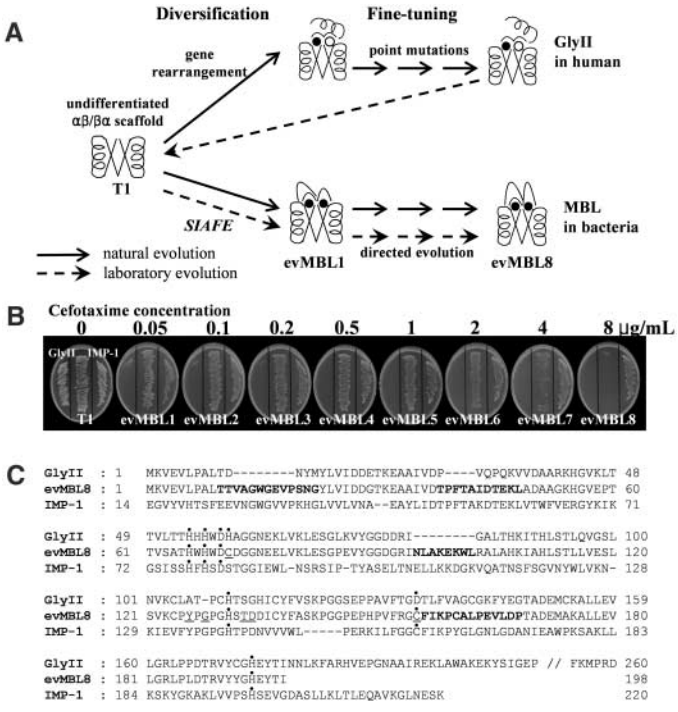

Fig. 3. Evolutionary trajectory of β-lactamase activity from the GlyII scaffold through SIAFE and directed evolution. (**A**) Schematic diagram showing the trajectories of the natural and artificial laboratory evolution of αβ/βα scaffold enzymes. (**B**) Cefotaxime resistance pattern of evolved enzymes selected at each round of evolution on selective plates with increasing concentrations of cefotaxime. (**C**) Sequence alignment of evMBL8 with GlyII and IMP-1. The specific mutations introduced by SIAFE are underlined, and newly designed loops are presented in bold. Residues essential for metal coordination are indicated with dots.

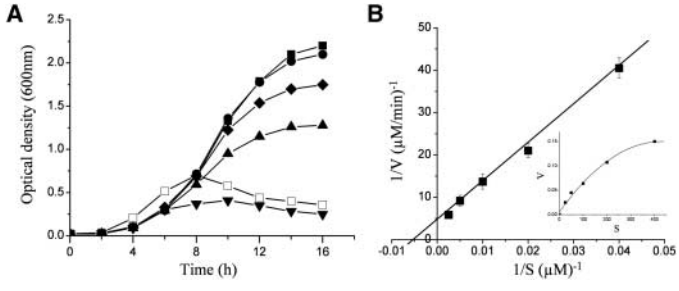

Fig. 4. Characteristics of evMBL8. (**A**) Growth patterns of *E. coli* cells with GlyII and evMBL8 on various cefotaxime concentrations. For evMBL8, cefotaxime concentrations are 0 (■), 0.2 (●), 0.5 (♦), 1.0 (▲), and 2.0 (▼) μg/ml. In the case of GlyII (□), the cefotaxime concentration was 0.02 μg/ml. (**B**) Steady-state kinetics (Lineweaver-Burke plot) of evMBL8 for cefotaxime.

Table 1. Kinetic constants and metal content of various enzymes.

Enzymes	k_{cat}* (s^{-1})	K_m* (μM)	k_{cat}/K_m ($M^{-1}s^{-1}$)	Metal (mol/mol of enzyme)*	
				Zn	Iron
GlyII	–	–	–	1.32 ± 0.27	0.10 ± 0.03
evMBL8	0.042 ± 0.003†	229 ± 36‡	1.84 × 10^2§	1.63 ± 0.43	0.46 ± 0.14
IMP-1	6.3 ± 0.8	7.9 ± 1.2	8.01 × 10^5	2.10 ± 0.50	–

*Values measured from at least three independent experiments †Apparent turnover number, k_{cat}^{app} ‡Apparent Michaelis-Menten constant, K_m^{app} §Apparent catalytic efficiency, $(k_{cat}/K_m)^{app}$

able variation among MBL family enzymes; accordingly, a mixture of three different oligonucleotides was used when designing this loop. Figure 2B shows the resulting loops: loop 1 (XXVXGWGXVPSNG), loop 2 (TPFTDXXTEKL), loop 4 (ELAKKXGX), and loop 6 (FIKAXXXGNXXDA, TLKAXXXGNXXDA, and XLKXXXAXXLGNXXDA). The loops contain residues that are in MBL family enzymes and several random residues for fine adjustment. The four sets of functional loops were incorporated into T2 with overlapping extension polymerase chain reaction (PCR) under error-prone conditions that also induce point mutations. Topology of the template scaffold GlyII and locations where the designed functional elements were incorporated are shown in fig. S2. The SIAFE approach allowed the constituents of the active site of GlyII to be replaced with newly designed functional elements in a planned and combinatorial manner. Mutation rates during mutagenic PCR were controlled at low levels (1 to 2 amino acid changes) and high levels (as many as 5 to 6 amino acid changes) throughout the gene to induce cumulative and synergistic effects on catalytic and substrate-binding sites.

From a library of 2.1 × 10^7 transformants, we first isolated 13 positive clones after two steps of selection on 0.2 μg/mL cefotaxime. All selected clones contained the segment (FIKAXXXGNXXDA) in loop 6 (fig. S3). Eight additional random mutations occurred in the active site loops. Further changes (2 to 9 amino acids) were randomly distributed in regions away from the active site. When functional elements were incorporated without additional mutations, no positive clones were isolated. The positive clones had undetectable β-lactamase activity. Thus, the isolated clones were subjected to directed evolution to increase their catalytic activities. Because the efficiency of directed evolution is highly dependent on the diversity of the starting clones, the library size was increased up to 1.5 × 10^8 with only the loop 6 segment (FIKAXXXGNXXDA). The resulting 312 positive clones were subjected to an additional seven rounds of directed evolution with DNA shuffling. To maintain high diversity, we selected positive clones from the library of more than 10^7 mutants at each round of in vitro evolution (table S1). As the evolution process progressed, selection pressure (cefotaxime concentration) was gradually increased from 0.2 to 4.5 μg/ml. In the seventh round of directed evolution, only 15 clones were isolated from the 7.0 × 10^7 mutant library at a cefotaxime concentration of 4.5 μg/ml. Of 15 positive clones, the one showing the most improved growth pattern on selective plates was selected. Additional rounds only resulted in a marginal increase in growth resistance for cefotaxime.

The overall evolution process to generate β-lactamase activity from template T1 is schematically represented in Fig. 3A. The figure also illustrates the trajectories of natural evolution and artificial laboratory evolution of the αβ/βα scaffold enzymes, GlyII and MBL. At the stage of SIAFE and each round of directed evolution, the clones showing the highest resistance against cefotaxime were selected as representatives and designated evMBL1 to evMBL8. The increasing resistance caused by these evMBL mutants was demonstrated by the comparison of growth between host cells expressing evolved enzymes and wild-type GlyII and IMP-1 on various dosages of cefotaxime (Fig. 3B). The observed growth resistance of evolved enzymes was somewhat higher than their actual resistance because of a confluence effect. Nonetheless, overall growth resistance of selected mutants gradually increased from 0.05 to 8 μg/ml, so antibiotic resistance was increased by a factor of about 160 through artificial evolution of the GlyII scaffold. The possibility of contamination by wild-type IMP-1 in the bacterial population carrying evMBL8 was checked and ruled out (*19*).

The amino acid sequence of the finally selected evMBL8 was determined and compared with those of GlyII and IMP-1 (Fig. 3C). Interestingly, evMBL8 carries only a 59% amino acid identity with GlyII, even though it has evolved from the GlyII scaffold. This indicates that 81 of the 198 amino acid residues were changed through insertion, deletion, and substitution of functional elements in addition to accumulation of point

mutations by SIAFE and directed evolution. Meanwhile, the amino acid sequence identity of evMBL8 with IMP-1 (25%) was almost double that of GlyII with IMP-1 (13%). As expected from the design strategy, more than 60% (49 amino acids) of mutations were concentrated in the catalytic and substrate-binding regions. In addition, many originally designed conserved residues in functional loops were changed during evolution. Nonetheless, the residues responsible for metal coordination (H66, H68, and H131 for metal 1; D70, C155, and H194 for metal 2) were not changed despite extensive mutagenesis. Replacement of any of these residues in evMBL8 with Ala resulted in loss of catalytic activity (*19*). Mutations C71H and C155D, which were attempts to restore GlyII-like metal coordination (H59 and D134) in evMBL8, also resulted in complete loss of catalytic activity (*19*). Thus, as evMBL8 evolved to have β-lactamase activity, it retained the designed metal coordination of IMP-1 that is essential for catalysis.

To further confirm the evolution of β-lactamase activity from the GlyII scaffold, evMBL8 was characterized in terms of in vivo biological activity, kinetic constants, and metal content. When *E. coli* cells expressing the evMBL8 were grown in liquid medium, distinct cell growth was observed up to cefotaxime concentrations of 1.0 μg/ml (Fig. 4A). A further increase in cefotaxime concentration (>2.0 μg/ml) caused a serious inhibition of cell growth due to cell lysis. On the other hand, cells expressing GlyII showed growth inhibition even at cefotaxime concentrations of 0.02 μg/ml. To study enzyme kinetics, evMBL8 was expressed as a fusion with maltose-binding protein (MBP) to improve stability (fig. S4). evMBL8 exhibited a typical saturation profile for cefotaxime, and k_{cat}^{app} and K_m^{app} were calculated to be 0.042 s^{-1} and 229 μM, respectively, from the reciprocal plot (Fig. 4B and Table 1). These values are lower by a factor of 150 and higher by a factor of 30 than the k_{cat} and K_m values of wild-type IMP-1, respectively, with the difference in K_m providing evidence against contamination by IMP-1 in conjunction with their relative activities for various substrates (table S2). Consequently, overall catalytic efficiency $(k_{cat}/K_m)^{app}$ of evMBL8 for cefotaxime was estimated to be 1.8×10^2 $M^{-1}s^{-1}$, which is about 3 to 4 orders of magnitude lower than that of wild-type IMP-1. Nonetheless, evMBL8 was active enough to provide *E. coli* cells a resistance against cefotaxime that is higher by a factor of 100 compared with cells having no evMBL8 (Fig. 4A). To check whether evMBL8 was still able to bind metal ions in its fused form with MBP, the total metal content of the enzyme was measured. Mutation H59C of GlyII was reported to cause a loss of zinc while maintaining iron content at a normal level, which suggests that H59C severely impaired the metal-binding site for zinc (*15*). However, evMBL8 with mutation H59C was found to bind both zinc (1.6 mol) and iron (0.4 mol) essential for hydrolytic reaction at levels comparable to GlyII (Table 1). It is likely that the disruption of metal coordination was reversed by other mutations during the directed evolution process.

Molecular modeling of evMBL8 with either an MBL family member (CcrA) or GlyII as the template gave an evMBL8 structure that is similar to that of the target IMP-1 (fig. S5A) but shows a distinct active site architecture compared with the template GlyII (fig. S5B). The model of the evMBL8-cefotaximne complex shows well-organized metal coordination (H66, H68, and H131 for metal 1; D70, C155, and H194 for metal 2) at the bottom of the active site (fig. S5C), which is consistent with the mutation study on putative metal ligands described above. Within the active site, loop 2 (T38-L48) and loop 6 (F156-P168) constitute two walls of the substrate-binding pocket, and loop 1 (T10-G22) forms the ceiling. Thus, we suggest that evMBL8 has acquired a new active site architecture with well-defined metal coordination and a substrate-binding pocket for new catalytic activity through the SIAFE and directed evolution process.

The design strategy presented here enabled the conversion of an enzyme in the metallohydrolase superfamily into a new family member with a different catalytic function, providing experimental support for the divergent evolution of mechanistically diverse family enzymes. We hope that the developed process can be extended to other scaffolds and create a larger variety of catalytic lineages performing diverse reactions and perhaps even reactions not found in nature.

References and Notes

1. S. J. Benkovic, S. Hammes-Schiffer, *Science* **301**, 1196 (2003).
2. F. H. Arnold, *Nature* **409**, 253 (2001).
3. A. Schmid *et al.*, *Nature* **409**, 258 (2001).
4. A. C. Joerger, S. Mayer, A. R. Fersht, *Proc. Natl. Acad. Sci. U.S.A.* **100**, 5694 (2003).
5. H. S. Park, K. H. Oh, H. S. Kim, *Methods Enzymol.* **388**, 187 (2004).
6. Y. H. Cheon *et al.*, *Biochemistry* **43**, 7413 (2004).
7. L. Tang *et al.*, *Biochemistry* **44**, 6609 (2005).
8. M. A. Dwyer, L. L. Looger, H. W. Hellinga, *Science* **304**, 1967 (2004).
9. S. Leopoldseder, J. Claren, C. Jurgens, R. Sterner, *J. Mol. Biol.* **337**, 871 (2004).
10. A. Aharoni *et al.*, *Nat. Genet.* **37**, 73 (2005).
11. H. Daiyasu, K. Osaka, Y. Ishino, H. Toh, *FEBS Lett.* **503**, 1 (2001).
12. A. D. Cameron, M. Ridderström, B. Olin, B. Mannervik, *Struct. Fold. Des.* **7**, 1067 (1999).
13. Z. Wang, W. Fast, A. M. Valentine, S. J. Benkovic, *Curr. Opin. Chem. Biol.* **3**, 614 (1999).
14. N. O. Concha *et al.*, *Biochemistry* **39**, 4288 (2000).
15. T. M. Zang *et al.*, *J. Biol. Chem.* **276**, 4788 (2001).
16. Z. Wang, W. Fast, S. J. Benkovic, *Biochemistry* **38**, 10013 (1999).
17. M. P. Yanchak, R. A. Taylor, M. W. Crowder, *Biochemistry* **39**, 11330 (2000).
18. S. D. Scrofani *et al.*, *Biochemistry* **38**, 14507 (1999).
19. Materials and methods are available as supporting material on *Science* Online.

20. We thank R. Sterner, M. Meyer, and F. Arnold for helpful comments, and J. H. Kim and S. C. Lee for technical assistance. Supported by National Research Laboratory program and Microbial Genomics and Application Center of Ministry of Science and Technology, Nano-Medical Project of Ministry of Health and Welfare, R & D program of Fusion Strategies for Advanced Technologies of Ministry of Commerce, Industry and Energy, and Brain Korea 21 of Ministry of Education and Human Resources Development, Korea.

Supporting Online Material

www.sciencemag.org/cgi/content/full/311/5760/535/DC1
Materials and Methods
SOM Text
Figs. S1 to S6
Tables S1 and S2
References

16 August 2005; accepted 7 December 2005
10.1126/science.1118953

A Virus Reveals Population Structure and Recent Demographic History of Its Carnivore Host

Roman Biek,[1]*† Alexei J. Drummond,[3] Mary Poss[1,2]

Directly transmitted parasites often provide substantial information about the temporal and spatial characteristics of host-to-host contact. Here, we demonstrate that a fast-evolving virus (feline immunodeficiency virus, FIV) can reveal details of the contemporary population structure and recent demographic history of its natural wildlife host (*Puma concolor*) that were not apparent from host genetic data and would be impossible to obtain by other means. We suggest that rapidly evolving pathogens may provide a complementary tool for studying population dynamics of their hosts in "shallow" time.

The genetic population structure of human pathogens often reflects known patterns of human migration (*1–4*). Moreover, the rapid evolutionary rate of many viral parasites means that this information can manifest itself over months or years (*5*). With HIV, for example, the origin and demographic history of epidemics have been determined retrospectively